Res Chem Intermed (2015) 41:5137–5147
DOI 10.1007/s11164-014-1617-6

Synthesis of Ag_3PO_4–AgBr with a novel heterostructure, and its photocatalytic properties

Xiufang Wang · Shizhen Yuan · Shaohua Chen · Guangmei Chen · Jun Zhang · Lei Zhang

Received: 5 December 2013 / Accepted: 13 March 2014 / Published online: 4 April 2014
© The Author(s) 2014. This article is published with open access at Springerlink.com

Abstract Ag_3PO_4–AgBr nanocomposites with a novel heterostructure were synthesized by a simple one-step reaction at room temperature with cetyltrimethylammonium bromide as surfactant and bromine source. The nanocomposites comprise uniform, monodisperse nanospheres of average diameter 90 nm. AgBr nanoparticles are present both on the surface and inside the nanospheres. The morphology of the composites can be controlled by adjusting the reaction conditions. The photocatalytic activity of the nanospheres was evaluated by monitoring degradation of methyl orange and rhodamine B under visible light irradiation. The results indicate that this novel heterostructure has much greater activity and structural stability than pure Ag_3PO_4. This may be primarily ascribed to effective separation of photoexcited electron–hole pairs at the contact interfaces.

Keywords Photocatalysis · Nanoparticles · Dyes · Silver phosphate · Silver bromide · Heterostructure

Introduction

Semiconductor photocatalysis is believed to have potential for solving environment pollution and energy problems [1–5]. Among photocatalysts, titanium dioxide (TiO_2) has proved to be the most promising and most effective material because of its photocatalytic activity, stability, and low toxicity. However, TiO_2 is a wide-band-gap energy semiconductor, active only under UV light irradiation. Development of new photocatalysts with high stability and high catalytic efficiency in sunlight is a fundamental issue in photocatalysis. Substantial progress was recently made by Ye and

X. Wang (✉) · S. Yuan · S. Chen · G. Chen · J. Zhang · L. Zhang
School of Materials and Chemical Engineering, Anhui Jianzhu University, Hefei 230601, People's Republic of China
e-mail: wxfrye159@sina.com

co-workers [6, 7], who reported novel use of an Ag_3PO_4 semiconductor which can make full use of visible light for evolution of O_2 from water and in the decomposition of organic dyes under visible light irradiation. They reported that the activity of Ag_3PO_4 was substantially higher than that of currently known visible light photocatalysts. However, it should be noted that this Ag_3PO_4 photocatalytic system still has limitations, for example, poor adsorptive performance, poor stability, and large particle size [6–8], the last of which affects the rate of migration of electron–hole pairs, thus affecting photocatalytic activity. It is, therefore, highly desirable to develop an effective method for improving the photocatalytic activity of Ag_3PO_4 photocatalysts.

Because the rate of recombination of photogenerated electrons and holes is reduced in composite semiconductors, these have been widely used to improve the photocatalytic activity of photocatalysts [9, 10]. Among a variety of composite materials, the heterojunction structure has been shown to be a very efficient method of separation of electron–hole pairs [11–13]. Photocatalysts with different types of heterostructure have been synthesized [14–18]. Bi et al. [19] reported a process for fabrication of Ag nanowire–Ag_3PO_4 cube necklace-like heterostructures with much higher activity than either pure Ag_3PO_4 cubes or Ag nanowire in the degradation of organic contaminants under visible light irradiation. Yao et al. [20] synthesized an Ag_3PO_4–TiO_2 visible light photocatalyst with better photocatalytic activity and stability than Ag_3PO_4. Xu et al. [21] prepared a heterojunction AgBr–$BiPO_4$ photocatalyst by a hydrothermal method and evaluated its photocatalytic activity by monitoring the degradation of methylene blue dye. Ye and co-workers [22] used an ion-exchange process for synthesis of uniform AgX–Ag_3PO_4 core–shell heterocrystals with rhombic dodecahedral structures. Hetero-photocatalysts are, however, usually obtained by random loading of nanoclusters on to semiconductor surfaces, which only facilitates surface separation of photoexcited electron–hole pairs rather than bulk-phase separation. The particle size of photocatalysts is also relatively large still, which hinders their performance in photocatalytic processes. To enhance photocatalytic activity, synthesis of nanosized Ag_3PO_4 particle-based hetero-photocatalysts with greater surface area and high photocatalytic efficiency is still a huge challenge.

Herein, we report facile one-step room-temperature fabrication of Ag_3PO_4–AgBr nanocomposites with a novel heterostructure, by use of cetyltrimethylammonium bromide (CTAB) as surfactant and source of bromine. The nanocomposites are uniform nanospheres of average diameter 90 nm, with AgBr nanoparticles both on the surface and inside the nanospheres. These Ag_3PO_4–AgBr nanocomposites with a special heterostructure have much greater photocatalytic activity and better stability than pure Ag_3PO_4 in the photodegradation of organic compounds. This may be primarily ascribed to effective separation of photoexcited electron–hole pairs at the contact interfaces.

Experimental

Materials

CTAB, Na_2HPO_4, and $AgNO_3$ were all analytical-grade reagents (Shanghai Chemical Reagent, China). Other reagents were used as received without further

purification. Double distilled water was used throughout the experiment to prepare the solutions.

Synthesis of Ag_3PO_4 crystals

Ag_3PO_4 was prepared by using silver-ammino complex as the source of silver ions. In a typical synthesis, aqueous ammonia solution (0.1 M) was added dropwise to an aqueous solution of $AgNO_3$ (0.05 M), to give a transparent solution. Aqueous Na_2HPO_4 solution (0.15 M) was then added, resulting in formation of Ag_3PO_4 crystals.

Synthesis of Ag_3PO_4–AgBr heterocrystals

Ag_3PO_4–AgBr heterocrystals were prepared by a simple precipitation process. In a typical synthesis, aqueous solutions of Na_2HPO_4 (0.5 mmol, 20 mL) and CTAB (0.5 mmol, 40 mL) were separately added dropwise to an aqueous solution $AgNO_3$ (2 mmol), giving a golden yellow precipitate. The precipitate was isolated by filtration, washed with deionized water and ethanol until the filtrate became colorless, and finally dried under vacuum at 60 °C for 24 h to obtain the Ag_3PO_4–AgBr nanocomposite as a dark powder (denoted Ag_3PO_4–AgBr-1).

To determine the effect of the amount of CTAB on the morphology and photocatalytic activity of the Ag_3PO_4–AgBr composites, a set of control experiments was performed with CTAB-to-Na_2HPO_4 molar ratios of 0.5, 4, to 8 (products denoted Ag_3PO_4–AgBr-2, Ag_3PO_4–AgBr-3 and Ag_3PO_4–AgBr-4, respectively) with the other synthetic conditions kept constant.

Photocatalytic reactions

The photocatalytic activity of the Ag_3PO_4–AgBr nanocomposites was evaluated by monitoring photocatalytic decolorization of dye solutions. The visible-light source was a 500-W xenon lamp positioned beside a cylindrical reaction vessel. A cutoff filter was placed inside the vessel to ensure complete removal of radiation below 420 nm and to ensure that irradiation of the Ag_3PO_4–AgBr system occurred at visible-light wavelengths only. The system was maintained at room temperature by use of a fan. The average light intensity was 30 mW cm^{-2}. Ag_3PO_4–AgBr nanocomposite (50 mg) was suspended in an aqueous solution (10^{-5} M; 50 mL) of the dye. To ensure establishment of an adsorption–desorption equilibrium among photocatalyst, dye, and water, the suspension was stirred continuously for approximately 30 min at room temperature. The stirred suspension was then exposed to visible light irradiation. The concentration of the dye was monitored by use of a model UV-4100 UV–visible spectrophotometer. Calibration, by use of the Beer–Lambert law, was at λ_{max} values of 553 and 463 nm for rhodamine B (RhB) and methyl orange (MO), respectively.

Characterization

SEM and FE-SEM images were obtained by use of a field-emission scanning electron microscope (JSM-7500F; Japan) operated at an accelerating voltage of 5 kV. X-ray diffraction spectra (XRD) were acquired by use of a Philips X'pert MPD instrument using Cu Kα radiation (50 kV). XRD patterns were recorded from 20° to 80° with a scanning rate of 0.067°/s. XPS was performed with an Escalab-MKII spectrometer (VG, UK) with Al Kr X-ray radiation as the X-ray source for excitation.

Results and discussion

Figure 1a shows a typical SEM image of as-prepared Ag_3PO_4 obtained without use of CTAB; it has an irregular spherical structure with non-uniform diameters. It is apparent from Fig. 1b that this sample has irregular polyhedral morphology. The morphology of the Ag_3PO_4–AgBr-1 nanocomposite is shown in Fig. 1c, which reveals the sample has a spherical heterostructure. The nanospheres are of average diameter 90 nm with narrow size distribution and excellent monodispersity. Figure 1d is a larger scale magnification of the SEM image of Ag_3PO_4–AgBr-1

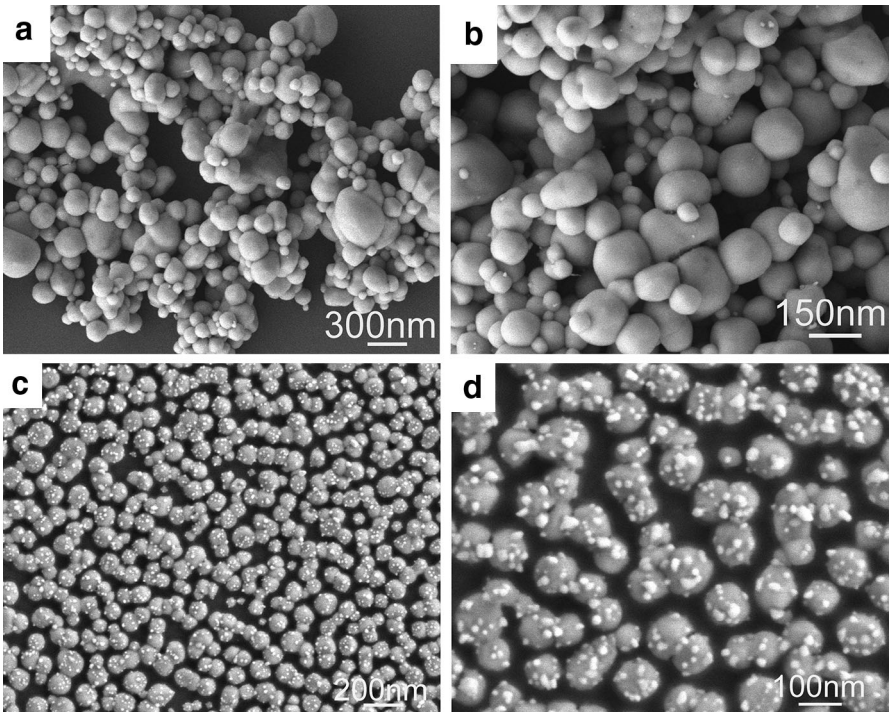

Fig. 1 SEM images of **a**, **b** Ag_3PO_4, and **c**, **d** Ag_3PO_4–AgBr-1 heterocrystals

nanospheres. Areas of darker color may be Ag_3PO_4 whereas the lighter areas are AgBr nanoparticles. The AgBr nanoparticles are distributed on the surface of Ag_3PO_4 nanospheres and some are wrapped by Ag_3PO_4, which indicates that AgBr and Ag_3PO_4 are generated at the same time.

Figure 2 shows X-ray diffraction patterns of as-prepared samples. Curves 1 and 2 are the XRD patterns of AgBr and Ag_3PO_4. Compared with the XRD pattern of pure Ag_3PO_4 crystals, that of Ag_3PO_4–AgBr-1 heterostructures contains Ag_3PO_4 reflection peaks (JCPDS. no. 06-0505) and AgBr reflection peaks (curves 3 and 4). The diffraction peaks marked "■" in curve 3 can be readily indexed as the (200), (220), and (400) planes of face-centered cubic (fcc) AgBr (JCPDS card no. 79-0149). This confirms the formation of Ag_3PO_4–AgBr composites.

XPS was performed to investigate the surface composition of Ag_3PO_4–AgBr-1 nanospheres. It is clear that the elemental content of the surface is Ag, P, O, and Br (Fig. 3a).The Ag 3d spectrum contains two peaks at ~374 and ~368 eV, which can be attributed to the Ag 3d3/2 and Ag 3d5/2 binding energies, respectively, suggesting the presence of Ag^+ (Fig. 3b). The P 2p XPS peak can be found at ca. 132 eV (Fig. 3c); this peak is ascribed to the P^{5+} in Ag_3PO_4 [23]. In Fig. 3d, the peak of Br 3d at 69 eV is because of the crystal lattice of Br^- in AgBr. Moreover, the XPS peak of O 1 s is at 531 eV, as shown in Fig. 3e [24]. The results from XRD, SEM, and XPS investigation confirm the presence of both Ag_3PO_4 and AgBr species in the heterojunction structure.

It is well known that synthetic conditions (for example the reaction temperature, concentration of reactants, and reaction time) affect the morphology and size of nanostructures. During this work it was found that the molar ratio of CTAB to Na_2HPO_4 (denoted *X*) had a crucial effect on the morphology of Ag_3PO_4–AgBr nanocomposites. Figure 4 shows a typical example of the effect of *X* on the morphology, as determined by use of SEM. When *X* is 0.5 the product is composed of approximately 90 nm Ag_3PO_4 nanospheres with AgBr nanoparticles on the surface of the nanospheres (Fig. 4a). When *X* is 4, the quantity of AgBr nanoparticles increases (Fig. 4b). If *X* is too high (>8), however, substantial agglomeration of the Ag_3PO_4–AgBr composite particles occurs (Fig. 4c). Thus, use of the correct molar ratio of CTAB to Na_2HPO_4 is crucial for formation of a uniform

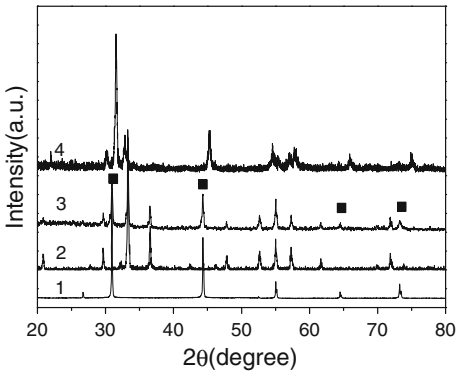

Fig. 2 XRD patterns of AgBr (*1*), Ag_3PO_4 (*2*), fresh Ag_3PO_4–AgBr-1 catalyst (*3*), and used catalyst (*4*)

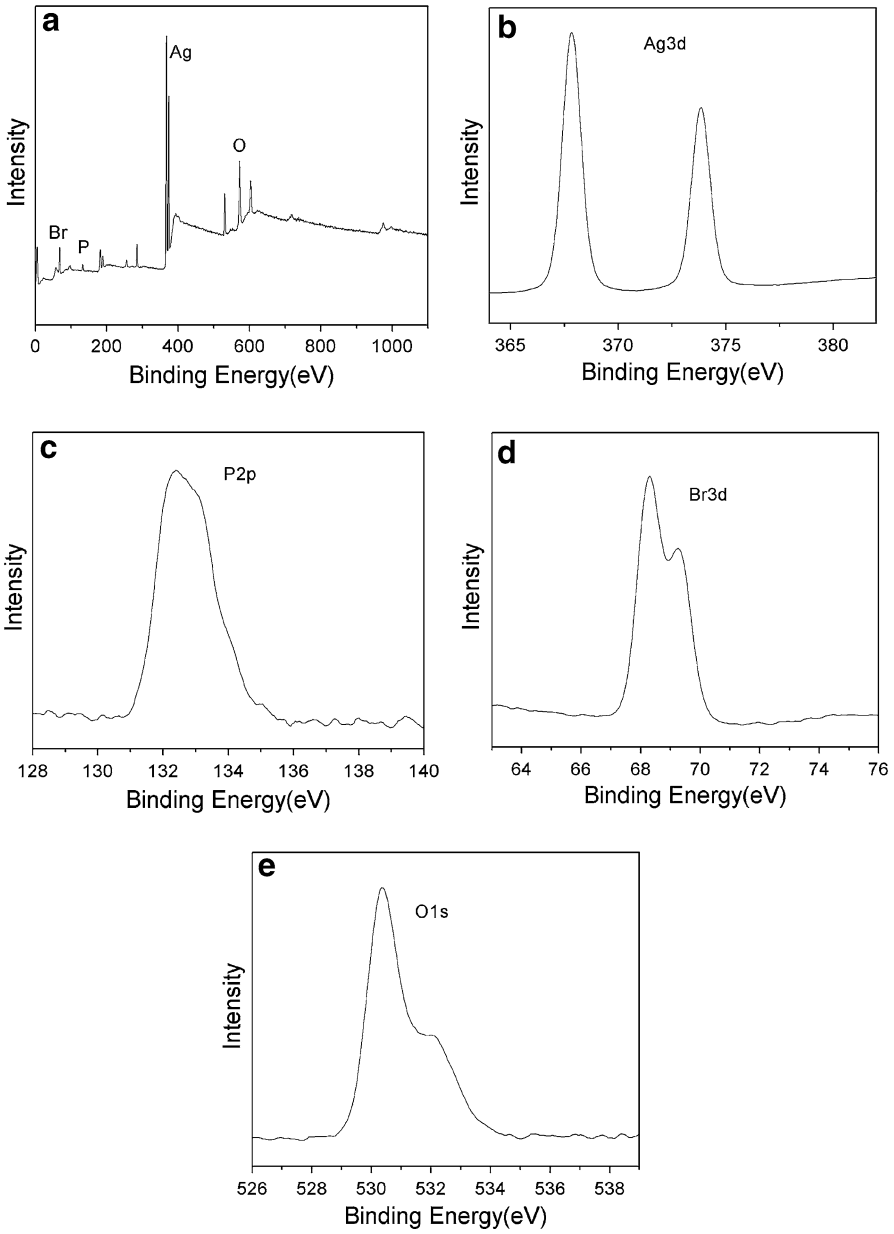

Fig. 3 XPS spectra of Ag_3PO_4–AgBr-1 heterocrystals. **a** Survey spectrum, **b** Ag 3d, **c** P 2p, **d** Br 3d, and **e** O 1s

Ag_3PO_4–AgBr heterostructure. On the basis of these results, it can be also concluded that CTAB, which is both surfactant and bromine source in this synthetic method, is important in determining the morphology of the Ag_3PO_4–AgBr.

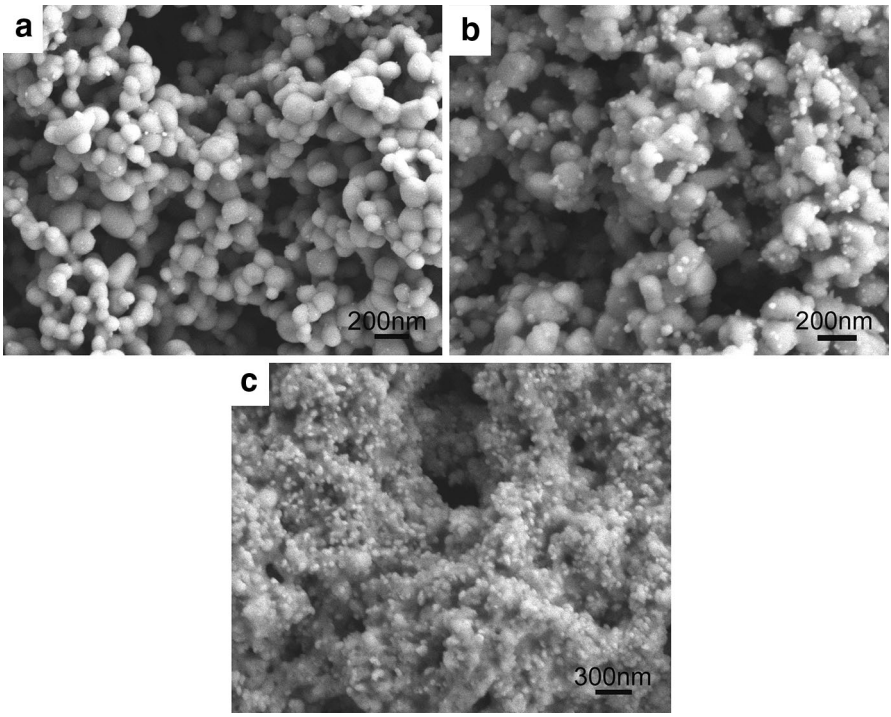

Fig. 4 SEM images of as-prepared Ag_3PO_4–AgBr heterostructures with different morphology obtained by use of CTAB-to-Na_2HPO_4 molar ratios of **a** 0.5, **b** 4, and **c** 8

The photocatalytic behavior of the as-prepared Ag_3PO_4–AgBr-1 heterostructure nanocomposites was investigated by monitoring the degradation of RhB dye under visible light irradiation at room temperature. RhB is relatively stable in aqueous solutions upon visible-light irradiation. Furthermore, photodegradation was not observed in the presence of Ag_3PO_4–AgBr-1 when the reaction mixture was maintained in darkness. Therefore, the illumination with light is necessary for efficient degradation, and the degradation of RhB is caused by photocatalytic reaction on Ag_3PO_4–AgBr-1. The characteristic absorption of RhB at $\lambda = 553$ nm was used to monitor the photocatalytic degradation process. Figure 5a shows the UV–visible absorption spectra of an aqueous solution of RhB at different times in the presence of Ag_3PO_4–AgBr-1 powder as photocatalyst. The absorption decreases rapidly with increasing exposure time, and completely disappears after approximately 4 min. The intense pink color of the starting RhB solution gradually fades during the process of photodegradation. The Ag_3PO_4–AgBr-1 catalyst has excellent photocatalytic activity.

The catalytic activity of the same sample of Ag_3PO_4–AgBr-1 nanocatalyst was tested five times in succession to evaluate renewal of the activity of the catalyst. Although there was a slight decrease in degradation efficiency, because of very slight dissolution of the Ag_3PO_4–AgBr-1 in the reaction solution, the efficiency of

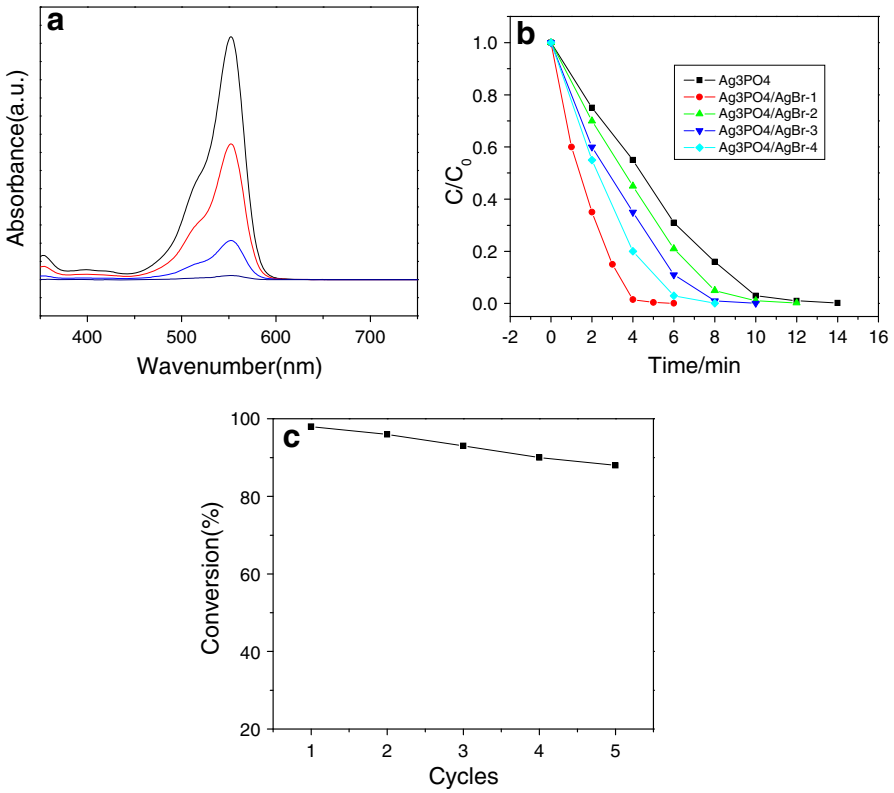

Fig. 5 **a** Absorption spectra of the RhB solution (1.0×10^{-5} M, 50 mL) in the presence of 50 mg Ag_3PO_4–AgBr-1 nanocomposite under exposure to visible light; **b** photodegradation of RhB by different photocatalysts; **c** degradation of RhB in five successive cycles with the same sample of Ag_3PO_4–AgBr-1 catalyst

degradation of RhB still reached 90 % after being recycled five times (Fig. 5c), indicating the composite photocatalyst has good photocatalytic stability. XRD of the used Ag_3PO_4–AgBr catalyst also reveals its stability (Fig. 2, curve 4).

For comparison, photodegradation of RhB was performed with the different samples under the same conditions. Among the samples, Ag_3PO_4–AgBr-1 heterocrystals had the highest photocatalytic activity. More specifically, with Ag_3PO_4–AgBr-1 the RhB dye was completely degraded in 4 min of visible light irradiation. Complete degradation of the RhB dye over the Ag_3PO_4–AgBr-2 photocatalyst took approximately 10 min whereas 8 min was needed when Ag_3PO_4–AgBr-3 was used. Ag_3PO_4–AgBr-4 was more active than Ag_3PO_4–AgBr-3; RhB was completely degraded in 6 min. With pure Ag_3PO_4, however, complete degradation of the RhB dye took nearly 16 min. These results clearly demonstrate that catalytic activity is related to structural features and the ratio of Ag_3PO_4 to AgBr.

To further test whether the Ag_3PO_4–AgBr-1 heterostructure nanocomposite had high photocatalytic activity in the degradation of pollutants, we investigated the

performance of Ag_3PO_4–AgBr-1 in the degradation of MO. Figure 6a shows the UV–visible absorption spectra of MO, with the increasing time, in the presence of Ag_3PO_4–AgBr-1 powder as photocatalyst. After 3 min the MO is degraded completely, indicating that Ag_3PO_4–AgBr-1 has high photocatalytic activity in the degradation of MO. Figure 6b shows the concentration of 4-chlorophenol (4-CP) at different times in the presence of Ag_3PO_4–AgBr-1 powder as photocatalyst. The Ag_3PO_4–AgBr-1 photocatalyst can also effectively degrade 4-chlorophenol (4-CP) under visible light irradiation.

The high photocatalytic performance of Ag_3PO_4–AgBr-1 heterocrystals can be attributed to the following characteristics:

1 The nanosized Ag_3PO_4–AgBr-1 particles have a large surface-to-volume ratio and more surface active sites, which are beneficial to diffusion and exchange of reaction intermediates.
2 The AgBr, which is poorly soluble, is in intimate contact with the outer surface of the Ag_3PO_4 crystals, preventing their dissolution. This enhances the structural stability of the catalyst;

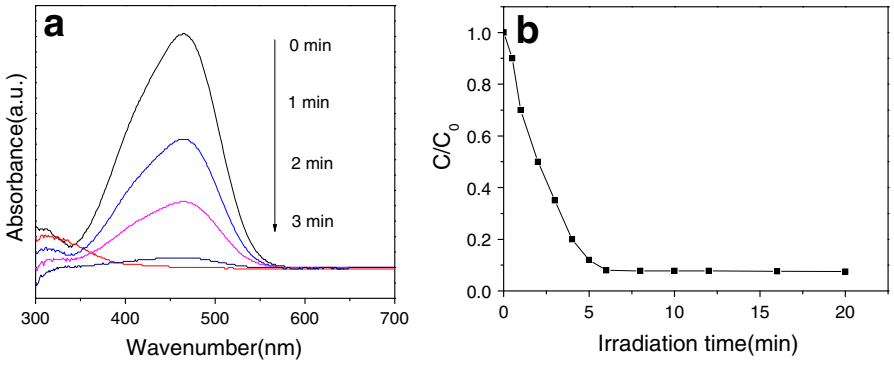

Fig. 6 Photodecomposition of MO (**a**) and 4-CP (**b**) by Ag_3PO_4–AgBr-1 under visible light irradiation

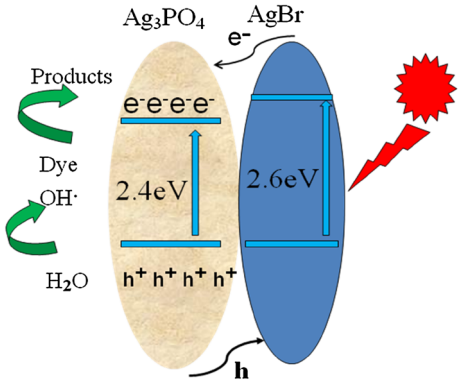

Fig. 7 Schematic diagram of the separation and transfer of photo-generated charge carriers in the Ag_3PO_4–AgBr system under visible light irradiation

3 The conduction band and valence band potentials of AgBr are more negative than those of Ag_3PO_4 (Fig. 7). As a result of the special heterostructure of the Ag_3PO_4–AgBr-1 catalysts, photogenerated electrons in the AgBr are readily transferred to the Ag_3PO_4 crystals, and the photoinduced holes on the surface of the Ag_3PO_4 can also migrate to AgBr, which promotes effective separation of photoexcited electron–hole pairs and reduces the probability of electron–hole recombination.

On the basis of the results presented, it can be concluded that the proposed fabrication of heterocrystals consisting of Ag_3PO_4 and AgBr is a successful and general strategy enabling development of highly active and stable photocatalysts under visible light irradiation.

Conclusions

In summary, Ag_3PO_4–AgBr heterojunction nanocrystals have been successfully synthesized by facile and efficient reaction at room temperature with CTAB as surfactant and bromine source. The nanocomposites are uniform, monodisperse nanospheres with an average diameter of 90 nm. In the degradation of organic contaminants under visible light irradiation the unique heterostructure of the Ag_3PO_4–AgBr resulted in greater photocatalytic activity and structural stability than for pure Ag_3PO_4. This is primarily ascribed to effective separation of photoexcited electron–hole pairs at the contact interfaces.

Acknowledgments This work was supported by the Natural Science Foundation of Anhui Province (1308085MB29), the Natural Science Foundation of China (21301004), and the College Students Innovative Training Program of Anhui Jianzhu University (201310878015).

Open Access This article is distributed under the terms of the Creative Commons Attribution License which permits any use, distribution, and reproduction in any medium, provided the original author(s) and the source are credited.

References

1. H. Zhang, G. Chen, D.W. Bahnemann, J. Mater. Chem. **19**, 5089 (2009)
2. Z. Kang, C.H.A. Tsang, N.B. Wong, Z. Zhang, S.T. Lee, J. Am. Chem. Soc. **129**, 12090 (2007)
3. H.T. Li, X.D. He, Z.H. Kang, H. Huang, Y. Liu, J.L. Liu, S.Y. Lian, S.T. Lee, Angew. Chem. Int. Ed. **49**, 4430 (2010)
4. S. Linic, P. Christopher, D.B. Ingram, Nat. Mater. **10**, 911 (2011)
5. Y. Liu, H. Ming, Z. Ma, H. Huang, S.Y. Lian, H.T. Li, X.D. He, H. Yu, K.M. Pan, Z.H. Kang, Chem. Commun. **47**, 8025 (2011)
6. Z.G. Yi, J.H. Ye, N. Kikugawa, T. Kako, S.X. Ouyang, H. Stuart-Williams, H. Yang, J.Y. Cao, W.J. Luo, Z.S. Li, Y. Liu, R.L. Withers, Nat. Mater. **9**, 559 (2010)
7. Y. Bi, S. Ouyang, N. Umezawa, J. Cao, J. Ye, J. Am. Chem. Soc. **133**, 6490 (2011)
8. Q.H. Liang, W.J. Ma, Y. Shi, Z. Li, X.M. Yang, Cryst. Eng. Commun. **14**, 2966 (2012)
9. H. Zhang, X. Fan, X. Quan, S. Chen, H. Yu, Environ. Sci. Technol. **45**, 5731 (2011)
10. Y.J. Wang, R. Shi, J. Lin, Y.F. Zhu, Energy Environ. Sci. **4**, 2922 (2011)

11. S.C. Yan, S.B. Lv, Z.S. Li, Z.G. Zou, Dalton Trans. **39**, 1488 (2010)
12. H. Xu, H.M. Li, C.D. Wu, J.Y. Chu, Y.S. Yan, H.M. Shu, Z. Gu, J. Hazard. Mater. **153**, 877 (2008)
13. M.L. Guan, D.K. Ma, S.W. Hu, Y.J. Chen, S.M. Huang, Inorg. Chem. **50**, 800 (2011)
14. M.S. Zhu, P.L. Chen, M.H. Liu, ACS Nano **5**, 4529 (2011)
15. R. Velmurugan, M. Swaminathan, Res. Chem. Intermed. **1**, 2495 (2013)
16. M.S. Zhu, P.L. Chen, M.H. Liu, Langmuir **28**, 3385 (2012)
17. M.S. Zhu, C.C. Chen, P.L. Chen, B. Lei, W.H. Ma, M.H. Liu, Phys. Chem. Chem. Phys. **15**, 12709 (2013)
18. M.S. Zhu, P.L. Chen, M.H. Liu, Langmuir **29**, 9259 (2013)
19. Y.P. Bi, H.G. Hu, S.X. Ouyang, Z.B. Jiao, G.G. Lu, J.H. Ye, J. Mater. Chem. **22**, 14847 (2012)
20. W.F. Yao, B. Zhang, C.P. Huang, C. Ma, X.L. Song, Q.J. Xu, J. Mater. Chem. **22**, 4050 (2012)
21. H. Xu, Y.G. Xu, H.M. Li, J.X. Xia, J. Xiong, S. Yin, C.J. Huang, H.L. Wan, Dalton Trans. **41**, 3387 (2012)
22. Y.P. Bi, S.X. Ouyang, J.Y. Cao, J.H. Ye, Phys. Chem. Chem. Phys. **13**, 10071 (2011)
23. C. Jin, R.Y. Zheng, Y. Guo, J.L. Xie, Y.X. Zhu, Y.C. Xie, J. Mol. Catal. A Chem. **313**, 44 (2009)
24. H. Zhang, G. Wang, D. Chen, X.J. Lv, J.H. Li, Chem. Mater. **20**, 6543 (2008)